Global neuronal activity drives cerebrospinal fluid motion mediated by brain blood volume changes in humans

Authors: Juliana Zimmermann[1,2,3]†, Clara Boudriot[1]†, Christiane Eipert[1]†, Gabriel Hoffmann[1], Rachel Nuttall[1,2], Sebastian Schneider[1,3], Lena Schmitzer[1], Jan Kufer[1], Stephan Kaczmarz[1], Dennis M Hedderich[1], Andreas Ranft[2], Daniel Golkowski[4,5], Josef Priller[6,7,8], Claus Zimmer[1], Rüdiger Ilg[4,9], Gerhard Schneider[2], Christine Preibisch[1,3,4], Christian Sorg[1,3,6]*‡, Benedikt Zott[1,10,11]*‡

Affiliations:

[1] Department of Neuroradiology, Technical University of Munich, School of Medicine, Munich, Germany

[2] Department of Anesthesiology and Intensive Care, Technical University of Munich, School of Medicine, Munich, Germany

[3] TUM-Neuroimaging Center, Technical University of Munich, School of Medicine, Munich, Germany

[4] Department of Neurology, Technical University of Munich, School of Medicine, Munich, Germany

[5] Department of Neurology, Heidelberg University Hospital, Heidelberg, Germany

[6] Department of Psychiatry and Psychotherapy, Technical University of Munich, School of Medicine, Munich, Germany

[7] Neuropsychiatry, Charité - Universitätsmedizin Berlin and DZNE, Berlin, Germany

[8] University of Edinburgh and UKI DRI, Edinburgh, UK

[9] Institute for Neuroscience, Technical University of Munich, Germany

[10] TUM Institute for Advanced Study, Garching, Germany

*Corresponding authors. Email: christian.sorg@tum.de, benedikt.zott@tum.de

† Equal contribution, ‡ Equal contribution

Abstract: Directed motion of cerebrospinal fluid (CSF flux) is instrumental for removing waste products from the brain. Fluctuations in global cerebral blood volume (CBV), induced by concerted changes of brain-wide neuronal activity, are suggested to drive CSF-flux. To test this hypothesis, we performed two related experiments in healthy humans, namely electro-encephalography and blood oxygenation level-dependent functional-MRI during burst-suppression anesthesia, and arterial spin labeling and functional-MRI during transient hypercapnia challenges. Changes in total CBV, induced by changes in instantaneous global neuronal activity during burst-suppression or brain blood flow during hyper-normocapnia transitions, cause opposite functional-MRI signal changes in the basal cisternae, marking CSF flux from and into the brain. This direct coupling of global neuronal activity, brain blood volume and CSF flux indicates a mechanism to enhance brain waste clearance.

One-Sentence Summary: Here we show that CSF flux is mediated by brain blood volume changes, which can be driven by global neuronal activity.

Main Text:

In the brain, the removal of waste products depends on the exchange of molecules between the cerebrospinal fluid (CSF) and the interstitial fluid (*1-3*). According to the glymphatic system hypothesis (*4*), CSF enters the brain via periarterial spaces, passes the astrocytic barrier, and drains the interstitial fluid into perivenous spaces via a convective flow. CSF flux is induced by, arterial motion (*1, 5, 6*) or rhythmic oscillatory processes such as heartbeat and respiration (*7-10*). However, accumulating evidence suggests that low frequency oscillations of global cerebral blood volume (CBV) constitute an additional driving force as evidenced by corelated global grey matter (gGM) and CSF-signal fluctuations (*11-14*). For example, under non-rapid eye movement (NREM) sleep conditions, functional magnetic resonance imaging (fMRI) signal fluctuations in both gGM and CSF-containing voxels of the bottom slices in the fourth ventricle were found to be closely coupled among each other and to the amplitude of slow-delta waves recorded via electro-encephalography (EEG) (*11*). This finding has prompted the hypothesis that global neuronal activity may be a driver of brain CBV changes, ultimately causing CSF flux (*11*).

The current study demonstrates direct experimental evidence for this hypothesis. Concerning the global nature of driving neuronal activity, burst-suppression states provide consummate conditions to test the influence of global cortical activity changes on CSF flux. While during sleep or wakefulness global brain activity is only partly changed, for example during slow-wave sleep the spatiotemporal patterns of neuronal activity changes are associated with transient cortical down-states across different but not all brain regions (*15*), anesthesia-induced burst-suppression states are constituted by sharp contrasts between global isoelectric suppression phases (i.e., minimal neuronal EEG-sensitive activity) and global burst phases (i.e., brain-wide high broadband-power activity). Burst-suppression transitions, then, are well suited to test global neuronal activity effects on CSF flux (*16*).

Second, with respect to a direct evidence for the mediating role of global CBV on CSF flux, one should consider that – in order to maintain a constant intracranial pressure - the sum of blood, brain and CSF volumes must be stable (*17*). Thus, an increase of total CBV would lead to an extrusion of CSF from the brain and a decrease of CBV would facilitate inflow (*18*). CBV can be locally modulated by neuronal stimulation (*19*) and globally by forced inspiration (*14*) or, in a more controlled way, by hypercapnic challenges i.e., transiently increased inspiratory CO_2-levels. Remarkably, hypercapnic challenges cause global vasodilation and thus global increases in cerebral blood flow (CBF) and CBV in animals (*20, 21*) and humans (*19*) and are accompanied by slight decreases in neuronal activity (*22, 23*).

Therefore, to study the effect of global neuronal activity transitions on CSF flux via brain CBV changes, we performed two related experiments. First, we used EEG-fMRI data acquired during anesthesia-induced burst-suppression states to measure global neuronal activity by EEG and - by means of fMRI - both the global blood oxygenation level dependent (BOLD) signal of grey matter and CSF signal at the level of the basal cisternae. We expected strongly anti-correlated signals from global GM and brainstem CSF voxels for both suppression-to-burst and burst-to-suppression transitions. In a second experiment, we subjected healthy individuals to a transient hypercapnia

challenge and used pseudo-continuous arterial spin labeling (pCASL) MRI to confirm its vasodilatory effect as well as fMRI to probe the coupling between global GM-BOLD signal and CSF motion through the basal cisternae as in the first experiment. We expected that the hyper-normocapnia-induced vasodilatory changes induce a signal behavior similar to that observed during the burst-suppression transitions, but with the critical differences that global CBV changes are induced by hypercapnia directly instead of changes in global neuronal activity.

Neuronal activity induces gGM BOLD and CSF signal changes in burst-suppression anesthesia

First, we tested the effects of global neuronal activity on gGM-BOLD and CSF signal under burst-suppression anesthesia. We used previously recorded data from healthy subjects (n = 20), who had been intubated and anesthetized with sevoflurane at different concentrations including one epoch of ~4,3%, resulting in the typical burst-suppression EEG-pattern in 17 subjects (*24-27*). fMRI and EEG data were co-registered in a 3T-MRI scanner (**Fig. 1A**). From the BOLD-fMRI data, we extracted signal from global grey matter as well as from CSF-containing voxels of the most caudal slice (slice 1) of the imaging volume (*11-13, 28, 29*), containing the premedullary, lateral and posterior cerebellomedullary basal cisternae (**Fig. 1B**). As previously described (*27*), even on the single subject level, the gGM-BOLD signal faithfully followed the burst-suppression pattern in the EEG with an expected delay, both for transitions from suppression to burst epochs, and for transitions from burst to suppression (**Fig. 1C**). In the CSF voxels of slice 1, we detected a positive peak, which was clearly related to the decrease of the gGM-BOLD signal at the end of each burst (**Fig. 1 C,E).** Remarkably, we also detected an inverse negative transient in the CSF voxels of slice 1, which was correlated with an increase of the gGM-BOLD signal (**Fig. 1 C,D**). During phases of stable gGM-BOLD signal, both during neuronal suppression epochs and during long bursts, the CSF signal was likewise unchanging (**Fig. S1**). Thus, for both transitions, we observed significant anticorrelations between gGM-BOLD and CSF signals (**Fig. 1F**), while during steady state burst or suppression epochs, the correlation was not significantly different from zero (**Fig. 1G**).

To exclude that the observed CSF signals in slice 1 were influenced by blood-flow through large vessels, we divided our CSF mask in two subregions, one containing the vertebral arteries and one devoid of blood vessels (**Fig. S2A**). Both areas showed similar and highly correlated signals, supporting that blood-flow through large vessels does not influence our finding (**Fig. S2B**).

Together, these data demonstrate that the rapid 'switching' of global cortical neuronal activity in burst-suppression anesthesia drives large changes in gGM-BOLD signal, which are associated with anticorrelated changes in CSF signal across the basal brain cisternae.

Global GM BOLD and CSF signal changes due to hypercapnia-induced vasodilation

Next, we investigated whether the experimental manipulation of CBV can drive CSF-flux. We utilized a controlled hypercapnic challenge design in healthy subjects (n=17) to induce transient cerebral vasodilation under awake resting-state conditions (*19*). Within a total scan duration of 900 sec, baseline periods of 180 sec alternated with hypercapnia periods of 180 sec (**Fig. 2A**). Hypercapnia was induced gradually by increasing the inspiratory CO_2 concentration to 5% over ~30 s. The maximal CO_2 concentration was kept stable for 180 sec before it was reduced back to zero over 30 s. (**Fig. 2A**). CBF and fMRI signal changes were acquired separately by optimized pCASL and BOLD-fMRI sequences.

In a first step, we evaluated pCASL MRI data for CBF to confirm the hemodynamic-vasodilatory effect of the hypercapnia challenge (**Fig. 2B**). CBF was high across the whole brain during periods of high inspiratory CO_2 compared to zero CO_2 conditions (**Fig. 2C, *top***), which is in line with previous studies (*19, 30, 31*). The time course of the global grey matter CBF (gGM-CBF) followed the levels of inspiratory CO_2, i.e. was relatively stable during baseline conditions, increased with the rise of CO_2, until it almost reached a plateau, before decreasing with falling CO_2 (**Fig. 2C, *bottom***). The gGM-CBF increased by 41.6 +/- 11.8% from normo- to hypercapnia and it decreased by 44.8 +/- 13% during the inverse transition (**Fig. 2 D,E**).

In a second step, we evaluated the fMRI data for gGM-BOLD and CSF signal in the same way as in the burst suppression experiments (**Fig. 3A**). Both on single subject (**Fig. S3**) and group levels (**Fig. 3B**), upon the onset of hypercapnia, gGM-BOLD signal increased from a stable baseline and almost reached a plateau during the time at which CO_2 was kept at 5%, before decreasing again following the drop of inspiratory CO_2 levels. In the CSF-containing voxels of slice 1, we detected a signal dip that co-occurred with the increase of gGM-BOLD signal (**Fig. 3C)**, and a positive peak associated with the decrease of gGM-BOLD signal (**Fig. 3D**). As for the first experiment, the gGM-BOLD and CSF signals were anticorrelated during both transition periods from normo- to hypercapnia (N→H) and from hyper- to normocapnia (H→N) (**Fig. 3E**). The relatively low temporal resolution (TRs of > 1.2 sec) of our fMRI sequence does not allow for the evaluation of the exact timing of gGM-BOLD and CSF signal changes during the transition phases; however, the direct manipulation of cerebrovascular processes by hypercapnia establish their causal relationship to CSF signals.

In summary, these results demonstrate that H→N and N→H transitions, respectively, induce gGM-BOLD signal changes, which couple inversely with CSF signal changes in the basal cisternae of the brainstem.

CSF in- and outflux mediated by changes in global brain blood volume

Finally, across both experiments of burst-suppression and transient hypercapnia, we analyzed the CSF signals with respect to indicators of flux direction using slice-sensitive fMRI analysis of fMRI-based CSF signals in the basal cisternae (**Fig. 4A**). In both experiments, we detected a transient increase in CSF signal intensity that occurred simultaneously to the gGM-BOLD signal drop (**Figs. 4 B,C**). In line with the previous study of Fultz et al. (*11*), the CSF signal amplitude decreased with increasing slice number in both experiments (**Fig. 4 B,C**) and more steeply in the burst-suppression experiment. This amplitude decrease is indicative of influx into the imaging volume, as water-protons ('spins'), which are unsaturated and hence hyperintense when entering the imaging volume, get increasingly saturated and thus hypointense by experiencing repeated radiofrequency pulses along slices above bottom slice 1 (*32*).

In experiment 1, during steady-state conditions, i.e., phases of quiescent suppression or during long bursts, the gGM-BOLD and CSF signals were relatively stable and did not show large transients (**Fig. S2**). However, analysis across several slices revealed that the CSF signal intensity of slice 1 was higher than that of slices 2 and 3, for both long bursts and long suppression phases (Fig. 4D**, Fig. S4**), possibly due to smaller influx events, caused by respiration or heartbeat (*8, 9*).

During the transition from suppression to burst or from normo- to hypercapnia, the transient signal dip in the fMRI-based CSF signal associated with an increase in gGM-BOLD signal was clearly detectable in slice 1 but largely attenuated in slices 2 and 3 in both experiments (**Fig. 4 E,F**). This

signal dip might reflect passage of attenuated CSF through slice 1, (*32*) as would be expected by extrusion of saturated CSF from the imaging volume (see discussion).

To further investigate whether the observed bidirectional changes in fMRI-based CSF signal intensity were associated with in- and outflux of CSF, we compared the traces of slice 1 CSF signal to the negative derivative of the gGM-BOLD signal (**Fig. S5**). In previous reports (*11, 13*), the CSF signal had close resemblance with a negative derivative of gGM-BOLD, in which negative values were set to zero, indicating that only influx of CSF could be detected. However, our analysis revealed that for both experiments, the correlation between the slice 1 CSF signal and the non-thresholded negative derivative of the gGM-BOLD was higher than the zero-thresholded version, indicating that the signals were caused by in-and outflux rather than only by influx (**Fig. S4**).

Together, these results provide strong evidence for the notion that total CBV changes associated with global neuronal activity or experimentally induced by a hypercapnic challenge cause bidirectional in- and outflux of CSF across the basal cisternae.

Discussion and conclusions

This study demonstrates that rapid switches from cortical quiescence to phases with bursts of strong global neuronal activity across a broad-spectrum during burst-suppression anesthesia induce large global changes in the gGM-BOLD-signal, which cause opposite in- or outflux of CSF. In addition, we provide evidence from hypercapnia experiments that similar gGM-BOLD and CSF signal changes during hyper- to normocapnia or normo- to hypercapnia transitions are associated with alternating changes in brain cerebral blood flow. Since it is well established that CBF changes go along with CBV changes (*19, 30, 31*), our results indicate that global CBV is an important mediator of CSF flux. Eventually, these observations lead us to a unified model of global neuronal activity changes and related brain CBV-induced flux of CSF into and out of the brain (**Fig. 4G**), expanding previous models based on CSF influx data only (Fultz et al 2019, Yang et al 2022).

To explain the model, we start with steady-state baseline conditions – such as ongoing suppression (***1***). Under these conditions, there are no large surges of CSF across the basal cisternae (**Fig. S1**). However, the CSF intensity in the lowest slice 1 is slightly higher than that of slice 2 (**Fig. S4**), likely due to a constant exchange with 'fresh' less saturated CSF at the edge of the imaging volume. This could be due to small inflow events caused, among others, by respiration and heartbeat (*8, 9*), which reached the lowest, but not the adjacent slices and could not be resolved due to lack of temporal resolution in our imaging paradigm. When global neuronal activity increases - as in the transition from suppression to burst (***2***) -, this rise causes an increase of brain CBV (**Fig. 3**). The less saturated CSF spins are extruded from slice 1 and replaced by more saturated spins from fluid inside the imaging volume, thus leading to a transient signal dip in slice 1 but not more cranial slices. It is important to note that a negative transient in slice 1, which, according to our model represents outflux, was not reported previously (*11-14, 28, 29*). However, these studies used experimental conditions such as slow-wave sleep or wakefulness with less pronounced changes of gGM-BOLD. During the burst, brain CBV remains elevated (***3***) and comparatively stable. Accordingly, steady-state conditions are established in the CSF, where again, fMRI signal intensity in slice 1 is higher than in slice 2. The instantaneous switch to neuronal suppression (***4***) causes a decrease in CBV and leads to a transient inflow of fresh unsaturated fluid from outside the imaging volume into the skull. This leads to a pronounced signal, which is most pronounced at slice 1 and largely attenuated in higher slices (**Fig. 4**, most likely, because of saturation of the entering CSF

spins by experiencing an increasing number of RF-pulses (*11*). After brain CBV has returned to baseline levels (***5***), a steady state is reached again.

It is important to note that the observed coupling of brain CBV changes to CSF in-and outflux are faithfully reproduced when total CBV is modulated, instead of by changes in global neuronal activity levels, by a hypercapnic challenge, which is not expected to increase neuronal firing (*22, 23*). Remarkably, upon the decrease of gGM-BOLD, the decay of signal amplitude associated with CSF influx (**Fig. 4B**) is less pronounced than in the burst suppression dataset (**Fig. 4C**). A likely explanation for this observation is that more pronounced hemodynamic changes were induced by the hypercapnic challenge leading to faster influx of CSF, penetrating deeper into the imaging volume before experiencing the first RF pulse (*11*).

The large surges of CSF flux observed in this study may facilitate brain waste clearance due to enhancing mixing and 'directed diffusion' or convective flow (*33*). If so, burst-suppression may represent a protective state in severe brain pathologies such as early onset infantile epilepsy (*34*), coma (*35*) or hypothermia (*36*). Moreover, medically-induced burst-suppression is used as a neuroprotective tool in severe epilepsy (*37*). This indicates that burst-suppression may be an inherent protective mechanism of the brain, which reduces the energy demand (*38*) and may facilitate the clearance of toxic metabolites by means of intermittent bursts of activity that trigger large surges of CSF flow. Under surgical anesthesia, burst-suppression states are not desired and associated with detrimental outcomes (*39*). It is, however, unclear whether this is due to the burst-suppression pattern itself or rather due to increased toxicity of elevated levels of anesthetic agents or higher susceptibility of the respective patients (*40*).

Under physiological conditions, similar yet less drastic fluctuations of gross neuronal activity can be detected, for example, in NREM sleep during slow waves or K-complexes (*15*) or in awake resting-state conditions (*41*), and may represent a physiological clearing state of the brain. Particularly, NREM-associated changes in gGM-BOLD signals are associated with large pulsatile inflow events of CSF across the 4th ventricle (*11, 12*), which, together with an enlargement of the perivascular spaces (*2, 42*) are expected to facilitate brain waste clearance. In fact, sleep deprivation is associated with defects of metabolic brain clearance (*43*) and disrupted sleep slow wave activity is associated with impaired memory consolidation and the buildup of β-amyloid (*44, 45*), the key pathological correlate of Alzheimer's disease (*46*). Conversely, enhancing brain waste clearance, for example, by hypercapnic challenges (*47*) may provide a safe and simple means to help mitigate the buildup of toxic substrates in neurodegenerative diseases (*2*) such as Alzheimer's disease.

In summary, our experiments provide direct evidence for tight mechanistic coupling between global neuronal activity, global brain blood flow and volume, as well as CSF flux, which might be harnessed to enhance brain waste clearance, both under physiological conditions or experimentally.

References and Notes

1. J. J. Iliff *et al.*, Cerebral arterial pulsation drives paravascular CSF-interstitial fluid exchange in the murine brain. *J Neurosci* **33**, 18190-18199 (2013).
2. L. Xie *et al.*, Sleep drives metabolite clearance from the adult brain. *Science* **342**, 373–377 (2013).

3. B. A. Plog, M. Nedergaard, The Glymphatic System in Central Nervous System Health and Disease: Past, Present, and Future. *Annual Review of Pathology: Mechanisms of Disease* **13**, 379-394 (2018).
4. L. Zhao, A. Tannenbaum, E. N. T. P. Bakker, H. Benveniste, Physiology of Glymphatic Solute Transport and Waste Clearance from the Brain. *Physiology* **37**, 349-362 (2022).
5. S. J. van Veluw *et al.*, Vasomotion as a Driving Force for Paravascular Clearance in the Awake Mouse Brain. *Neuron* **105**, 549-561.e545 (2020).
6. H. Mestre *et al.*, Flow of cerebrospinal fluid is driven by arterial pulsations and is reduced in hypertension. *Nature Communications* **9**, 4878 (2018).
7. J. M. Spijkerman *et al.*, Phase contrast MRI measurements of net cerebrospinal fluid flow through the cerebral aqueduct are confounded by respiration. *Journal of Magnetic Resonance Imaging* **49**, 433-444 (2019).
8. V. Kiviniemi *et al.*, Ultra-fast magnetic resonance encephalography of physiological brain activity - Glymphatic pulsation mechanisms? *J Cereb Blood Flow Metab* **36**, 1033-1045 (2016).
9. S. Dreha-Kulaczewski *et al.*, Inspiration is the major regulator of human CSF flow. *J Neurosci* **35**, 2485-2491 (2015).
10. N. Alperin, E. M. Vikingstad, B. Gomez-Anson, D. N. Levin, Hemodynamically independent analysis of cerebrospinal fluid and brain motion observed with dynamic phase contrast MRI. *Magnetic resonance in medicine* **35**, 741-754 (1996).
11. N. E. Fultz *et al.*, Coupled electrophysiological, hemodynamic, and cerebrospinal fluid oscillations in human sleep. *Science* **366**, 628-631 (2019).
12. D. Picchioni *et al.*, Autonomic arousals contribute to brain fluid pulsations during sleep. *NeuroImage* **249**, 118888 (2022).
13. H.-C. Yang *et al.*, Coupling between cerebrovascular oscillations and CSF flow fluctuations during wakefulness: An fMRI study. *Journal of Cerebral Blood Flow & Metabolism* **42**, 1091-1103 (2022).
14. Y. Wang *et al.*, Cerebrovascular activity is a major factor in the cerebrospinal fluid flow dynamics. *NeuroImage* **258**, 119362 (2022).
15. S. S. Cash *et al.*, The Human K-Complex Represents an Isolated Cortical Down-State. *Science* **324**, 1084-1087 (2009).
16. A. Shanker, J. H. Abel, G. Schamberg, E. N. Brown, Etiology of Burst Suppression EEG Patterns. *Frontiers in Psychology* **12**, (2021).
17. B. Mokri, The Monro–Kellie hypothesis. *Applications in CSF volume depletion* **56**, 1746-1748 (2001).
18. N. Alperin, S. H. Lee, A. Sivaramakrishnan, S. G. Hushek, Quantifying the effect of posture on intracranial physiology in humans by MRI flow studies. *Journal of magnetic resonance imaging : JMRI* **22**, 591-596 (2005).
19. H. Ito, I. Kanno, M. Ibaraki, J. Hatazawa, S. Miura, Changes in Human Cerebral Blood Flow and Cerebral Blood Volume during Hypercapnia and Hypocapnia Measured by Positron Emission Tomography. *Journal of Cerebral Blood Flow & Metabolism* **23**, 665-670 (2003).
20. A. K. Olsen, S. Keiding, O. L. Munk, Effect of hypercapnia on cerebral blood flow and blood volume in pigs studied by positron emission tomography. *Comp Med* **56**, 416-420 (2006).
21. C. Z. Cooley, J. B. Mandeville, E. E. Mason, E. T. Mandeville, L. L. Wald, Rodent Cerebral Blood Volume (CBV) changes during hypercapnia observed using Magnetic Particle Imaging (MPI) detection. *Neuroimage* **178**, 713-720 (2018).

22. A. C. Zappe, K. Uludağ, A. Oeltermann, K. Uğurbil, N. K. Logothetis, The Influence of Moderate Hypercapnia on Neural Activity in the Anesthetized Nonhuman Primate. *Cerebral Cortex* **18**, 2666-2673 (2008).
23. C. Martin, M. Jones, J. Martindale, J. Mayhew, Haemodynamic and neural responses to hypercapnia in the awake rat. *European Journal of Neuroscience* **24**, 2601-2610 (2006).
24. D. Golkowski *et al.*, Changes in Whole Brain Dynamics and Connectivity Patterns during Sevoflurane- and Propofol-induced Unconsciousness Identified by Functional Magnetic Resonance Imaging. *Anesthesiology* **130**, 898-911 (2019).
25. D. Golkowski *et al.*, Coherence of BOLD signal and electrical activity in the human brain during deep sevoflurane anesthesia. *Brain and Behavior* **7**, e00679 (2017).
26. A. Ranft *et al.*, Neural Correlates of Sevoflurane-induced Unconsciousness Identified by Simultaneous Functional Magnetic Resonance Imaging and Electroencephalography. *Anesthesiology* **125**, 861-872 (2016).
27. N. Sirmpilatze *et al.*, Spatial signatures of anesthesia-induced burst-suppression differ between primates and rodents. *eLife* **11**, e74813 (2022).
28. F. Han *et al.*, Decoupling of Global Brain Activity and Cerebrospinal Fluid Flow in Parkinson's Disease Cognitive Decline. *Movement Disorders* **36**, 2066-2076 (2021).
29. F. Han *et al.*, Reduced coupling between cerebrospinal fluid flow and global brain activity is linked to Alzheimer disease–related pathology. *PLOS Biology* **19**, e3001233 (2021).
30. M. J. Donahue *et al.*, Bolus Arrival Time and Cerebral Blood Flow Responses to Hypercarbia. *Journal of Cerebral Blood Flow & Metabolism* **34**, 1243-1252 (2014).
31. D. F. Heijtel *et al.*, Accuracy and precision of pseudo-continuous arterial spin labeling perfusion during baseline and hypercapnia: a head-to-head comparison with ^{15}O H_2O positron emission tomography. *Neuroimage* **92**, 182-192 (2014).
32. J.-H. Gao, H.-L. Liu, Inflow effects on functional MRI. *NeuroImage* **62**, 1035-1039 (2012).
33. M. Asgari, D. de Zélicourt, V. Kurtcuoglu, Glymphatic solute transport does not require bulk flow. *Scientific Reports* **6**, 38635 (2016).
34. S. Ohtahara, Y. Ohtsuka, Y. Yamatogi, E. Oka, The early-infantile epileptic encephalopathy with suppression-burst: developmental aspects. *Brain Dev* **9**, 371-376 (1987).
35. E. N. Brown, R. Lydic, N. D. Schiff, General anesthesia, sleep, and coma. *N Engl J Med* **363**, 2638-2650 (2010).
36. M. B. Westover *et al.*, The human burst suppression electroencephalogram of deep hypothermia. *Clin Neurophysiol* **126**, 1901-1914 (2015).
37. A. O. Rossetti, D. H. Lowenstein, Management of refractory status epilepticus in adults: still more questions than answers. *Lancet Neurol* **10**, 922-930 (2011).
38. S. Ching, P. L. Purdon, S. Vijayan, N. J. Kopell, E. N. Brown, A neurophysiological–metabolic model for burst suppression. *Proceedings of the National Academy of Sciences* **109**, 3095-3100 (2012).
39. J. C. Pedemonte *et al.*, Electroencephalogram Burst-suppression during Cardiopulmonary Bypass in Elderly Patients Mediates Postoperative Delirium. *Anesthesiology* **133**, 280-292 (2020).
40. Y. R. Shao *et al.*, Low Frontal Alpha Power Is Associated With the Propensity for Burst Suppression: An Electroencephalogram Phenotype for a "Vulnerable Brain". *Anesthesia and analgesia* **131**, 1529-1539 (2020).

41. A. Mitra *et al.*, Spontaneous infra-slow brain activity has unique spatiotemporal dynamics and laminar structure. *Neuron* **98**, 297-305. e296 (2018).
42. L. Bojarskaite *et al.*, Sleep cycle-dependent vascular dynamics enhance perivascular cerebrospinal fluid flow and solute transport. *bioRxiv*, 2022.2007.2014.500017 (2022).
43. P. K. Eide, V. Vinje, A. H. Pripp, K.-A. Mardal, G. Ringstad, Sleep deprivation impairs molecular clearance from the human brain. *Brain* **144**, 863-874 (2021).
44. B. Zott, M. A. Busche, R. A. Sperling, A. Konnerth, What Happens with the Circuit in Alzheimer's Disease in Mice and Humans? *Annu Rev Neurosci* **41**, 277-297 (2018).
45. B. A. Mander *et al.*, beta-amyloid disrupts human NREM slow waves and related hippocampus-dependent memory consolidation. *Nat Neurosci* **18**, 1051–1057 (2015).
46. D. J. Selkoe, J. Hardy, The amyloid hypothesis of Alzheimer's disease at 25 years. *EMBO Mol Med* **8**, 595–608 (2016).
47. U. S. Yezhuvath, K. Lewis-Amezcua, R. Varghese, G. Xiao, H. Lu, On the assessment of cerebrovascular reactivity using hypercapnia BOLD MRI. *NMR Biomed* **22**, 779-786 (2009).
48. Y. Chao-Gan, Z. Yu-Feng, DPARSF: A MATLAB Toolbox for "Pipeline" Data Analysis of Resting-State fMRI. *Frontiers in systems neuroscience* **4**, 13 (2010).
49. J. Ashburner, A fast diffeomorphic image registration algorithm. *Neuroimage* **38**, 95-113 (2007).
50. D. C. Alsop *et al.*, Recommended implementation of arterial spin-labeled perfusion MRI for clinical applications: A consensus of the ISMRM perfusion study group and the European consortium for ASL in dementia. *Magn Reson Med* **73**, 102-116 (2015).

Acknowledgments:

Funding:

German Research Foundation (395030489) - CS and CP

German Research Foundation (DFG SFB/TRR167 B07) - JP.

BZ is a is an Albrecht-Struppler-Clinician Scientist Fellow, funded by the Federal Ministry of Education and Research (BMBF) and the Free State of Bavaria under the Excellence Strategy of the Federal Government and the Länder, as well as by the Technical University of Munich - Institute for Advanced Study.

Author contributions:

Conceptualization: JZ, CS, BZ

Investigation sevoflurane dataset: JZ, CB, CE, SS, GS, AR, RI, DG, RN, DMH, JP, CS, BZ

Investigation hypercapnia dataset: JZ, CB, CE, GH, RN, LS, JK, SS, LS, JK, SK, CZ, CP, CS, BZ

Visualization: JZ, CB, CE; GH, CS, BZ

Funding acquisition: CZ, CP, CS, BZ

Supervision: CP, CS, BZ

Writing – original draft: JZ, CB, CE, CP, CS, BZ

Writing – review & editing: all authors

Competing interests: Authors declare that they have no competing interests.

Data and materials availability: All data will be made available by the corresponding authors upon reasonable request.

Supplementary Materials

Materials and Methods

Figs. S1 to S5

References (*48–50*)

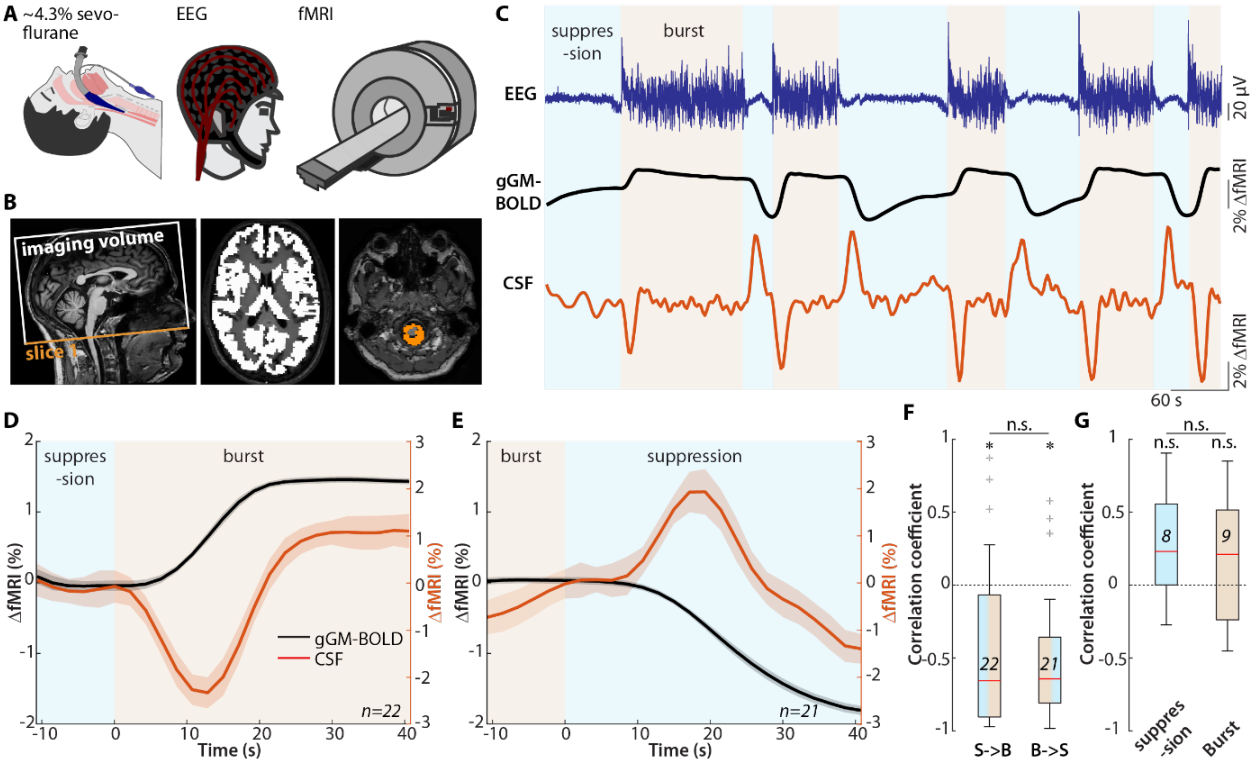

Fig. 1. Coupled neuronal activity, gGM-BOLD and CSF signals during burst-suppression anesthesia. (**A**) Experimental design: Under deep sevoflurane anesthesia, EEG and fMRI data was co-registered. (**B**) Example scan positioning in a representative subject. Schematic depiction of the fMRI imaging volume superimposed on a sagittal T1-weighted image (left). The position of slice 1 is indicated in *orange*. Grey matter mask in a representative axial slice *(middle)*. CSF mask in slice 1 *(right)*. (**C**) Representative EEG (*top, blue*), gGM-BOLD (*middle, black*) and CSF (*bottom, red*) signal time courses from one subject. Suppression and burst periods are indicated in light blue and light orange, respectively. (**D**) Subject- and event-averaged time courses of all transitions from suppression to burst (*n=22 events from 17 subjects*). gGM-BOLD (*black*) and CSF (*red*). The shaded areas represent standard error of the mean (SEM). Suppression and burst periods are indicated in light blue and light orange, respectively. (**E**) Same as (D) for transitions from burst to suppression (*n = 21*). (**F**) Correlation coefficients between gGM-BOLD and CSF signals during the transitions from suppression to burst (*S→B, left*) and burst to suppression (*B→S, right*). (**G**) Same as (F) for steady state suppression and steady state burst. *p<0.05, n.s. not significant. One-sample-t-test (individual groups), two-sample t-test (between groups).

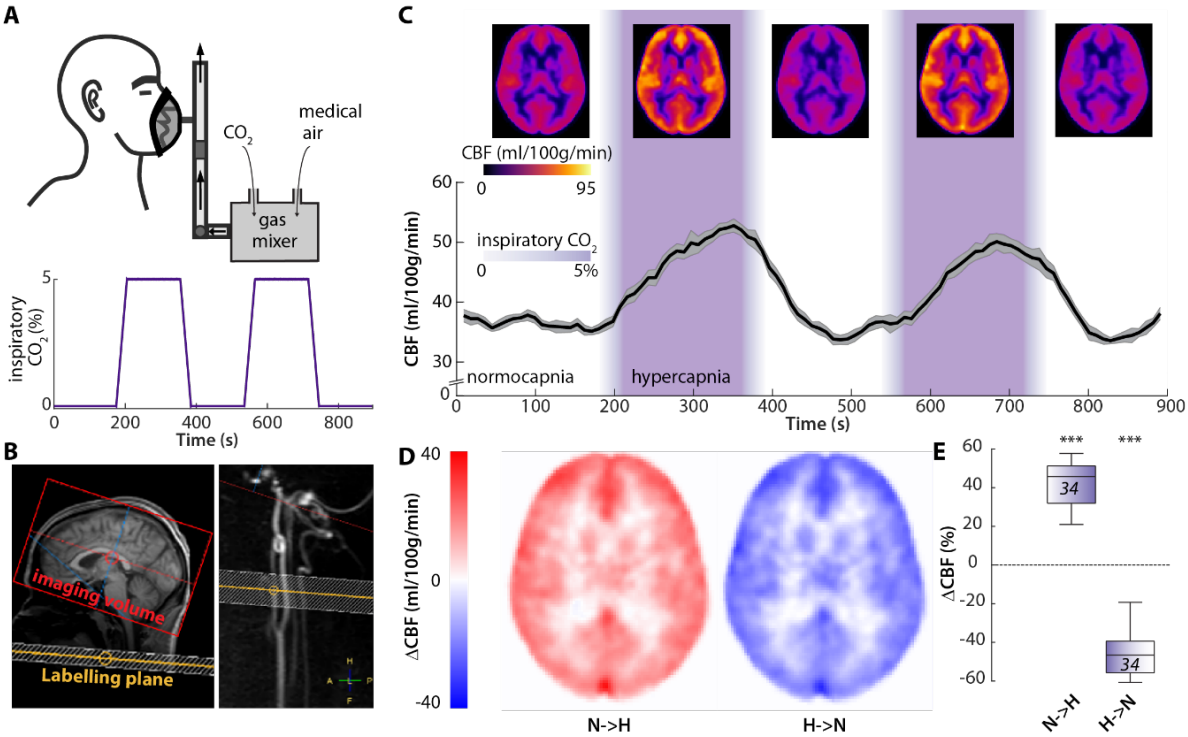

Fig. 2. Bidirectional grey-matter CBF changes induced by a hypercapnic challenge. (**A**) Schematic depiction of the experimental design: a gas mixture of CO_2 and medical air was applied over a medical mask in awake subjects *(top)*. Schematic time course of the inspiratory CO_2 concentrations contents of the applied gas mixture including two 180 s segments with elevated CO_2 levels (5% Vol/vol). Transition periods lasted ~30s due to ramp time of the gas mixer. (**B**) Example scan positioning for the pCASL imaging volume (red) and labeling plane (yellow) in a representative subject, superimposed on a sagittal T1 image (*left)* and a sagittal reconstruction of a 3D-phase contrast angiogram (*right*). (**C**) Whole brain cerebral blood flow (CBF) maps (*top*) and extracted subject-average (n = 17) time course of gGM CBF (*bottom*). Mean (*black*) ± SEM (*grey*). CO_2 application periods are color-coded in *purple*. (**D**) Subject-average maps of CBF changes (ΔCBF) for transitions from normocapnia to hypercapnia *(N→H, left)* or from hypercapnia to normocapnia (H→N, *right*). (**E**) Global grey matter ΔCBF values for *N→H, (n =34, left)* or *H→N (n =34, right) transitions* (2 for each subject). One-sample t-test (individual groups). ***p<0.001.

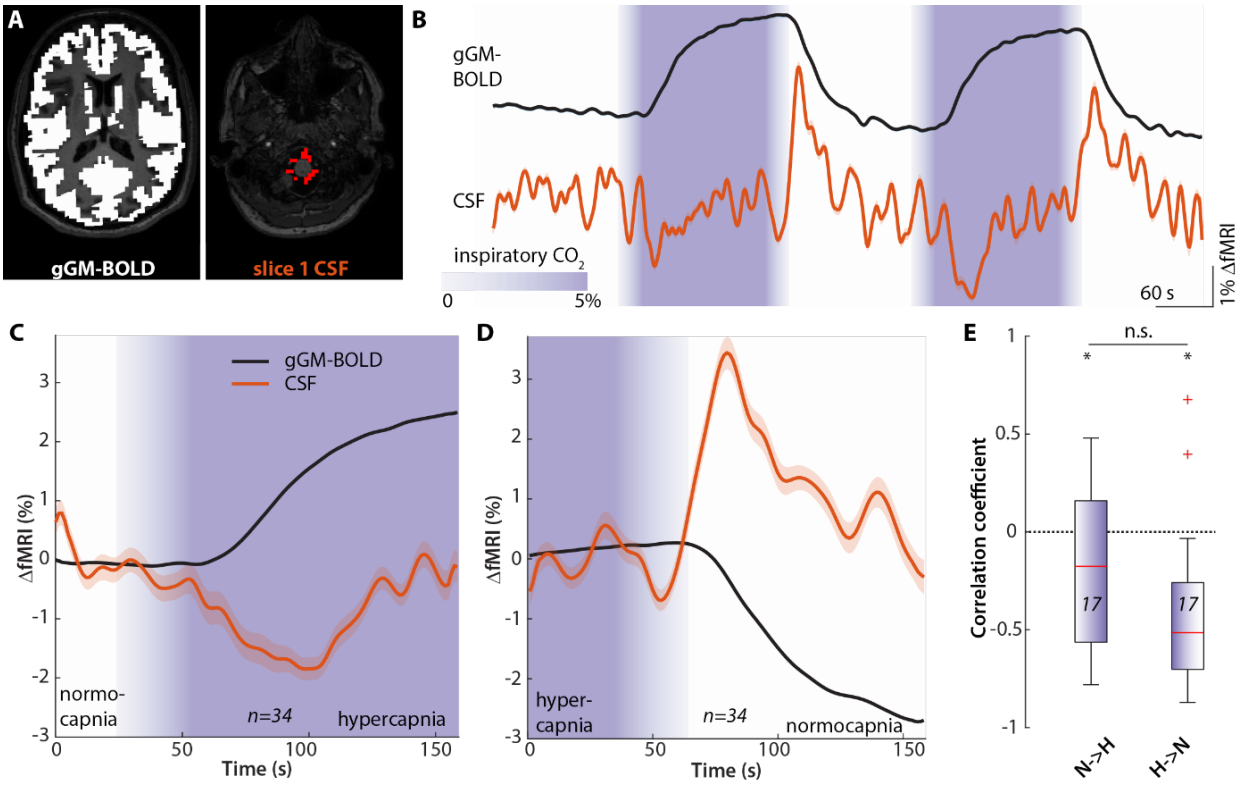

Fig. 3. Coupled gGM-BOLD and CSF signal changes induced by a transient hypercapnia challenge. (**A**) Grey matter (*left*) and CSF masks *(right) for extracting fMRI signals,* superimposed on axial T1-weighted images. (**B**) Time courses of the gGM-BOLD *(top, black)* and CSF *(bottom, red)* signals. Mean (*solid lines*) ± SEM (*shaded areas*) of n = 17 subjects. CO_2 application periods are color-coded in purple. (**C**) Averaged time courses of all normocapnia to hypercapnia (N→H) transitions (n = 34 transitions from 17 subjects). gGM-BOLD *(black)* and CSF signal *(red)*. The shaded areas represent SEM. CO_2 application periods are color coded in purple. (**D**) Same as (C) for transitions from hypercapnia to normocapnia (H→N, n = 34 transitions from 17 subjects). (**E**) Correlation coefficients between gGM-BOLD and CSF signals during N→H *(n=17, left)* and H→N *(n=17, right)* transitions. *p<0.05, n.s. not significant. One-sample t-test (individual groups). Two-sample t-test (between groups).

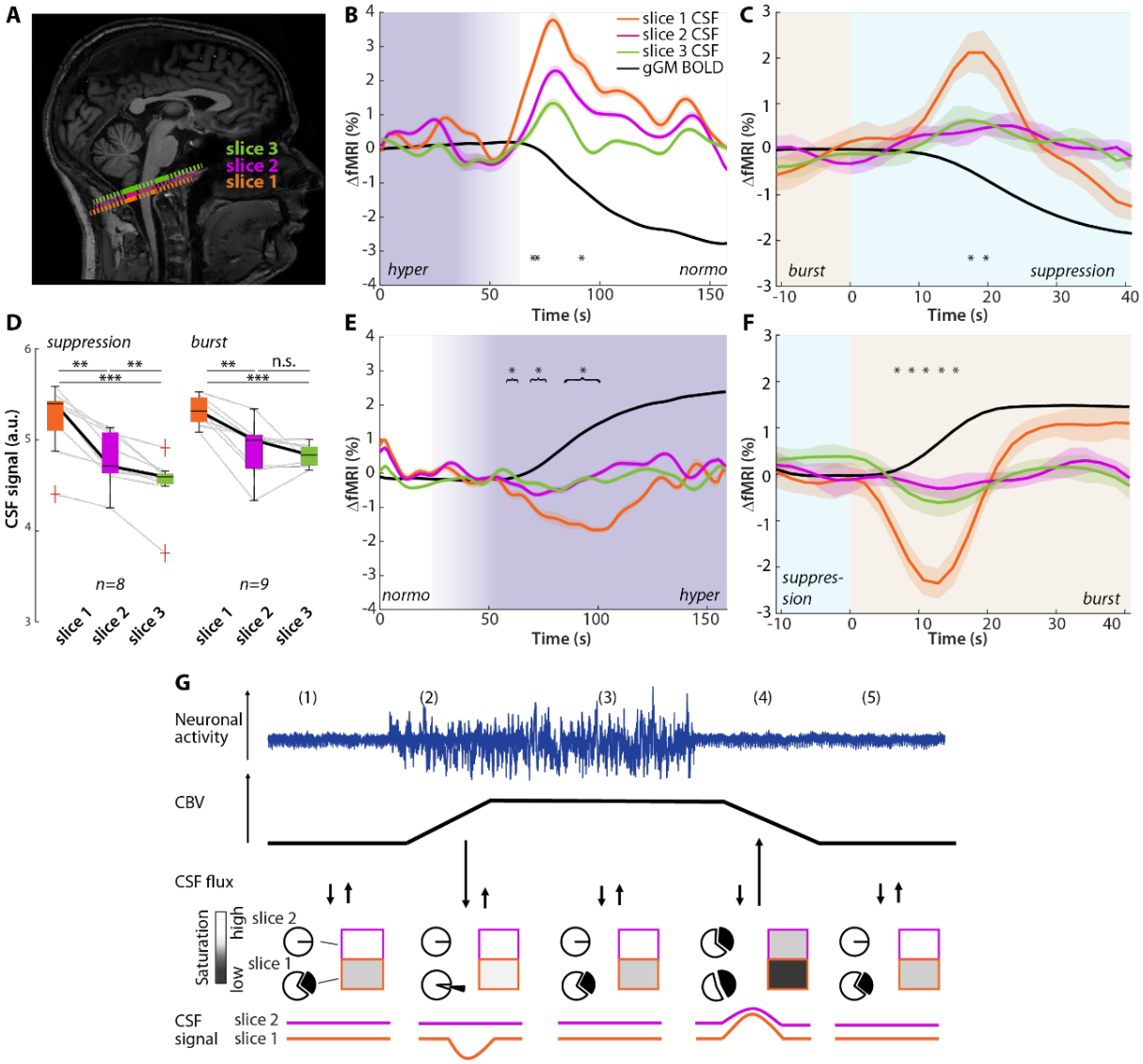

Fig. 4. Changes in global brain blood volume mediate CSF in- and outflux. (A) Representative example of the positioning of the most caudal fMRI slices on a sagittal T1-weighted image. The CSF voxels of slice 1 are indicated in *red*, slice 2 in *pink* and slice 3 in *green,* the dashed lines are schematic depictions of the respective imaging slices. (**B)** Average time courses of all transitions from hypercapnia to normocapnia. gGM-BOLD (*black*), CSF signal in slice 1 (*orange*), slice 2 (*pink*) and slice 3 (*green*). The shaded areas represent SEM. Hypercapnia and normocapnia periods are indicated in purple. *p<0.05, repeated-measures ANOVA (between slices) per subject (n=17). **(C)** Average time courses of all transitions from burst to suppression. Global GM-BOLD (*black*), CSF signal in slice 1 (*orange*), slice 2 (*pink*) and slice 3 (*green*). The shaded areas represent SEM. Burst and suppression periods are indicated in light orange and light blue, respectively. *p<0.05, repeated-measures ANOVA (between slices) per event (n=21). (**D)** Mean fMRI-based CSF signal intensities (a.u.) per event of slices 1-3 for steady state suppression or steady state burst periods. ** p<0.005, ***p<0.001, n.s. not significant. Repeated measures ANOVA with Dunn-Sidak post-hoc comparison. (**E)** Same as (B) for all transitions from normocapnia to hypercapnia. *p<0.05, repeated-measures ANOVA (between slices) per subject (n=17). (**F)** Same as (C) for all transitions from suppression to burst. ** p<0.005, ***p<0.001, repeated-measures ANOVA (between slices) per event (n=22). **(G)** Schematic model of the link between neuronal activity (*blue*), CBV (*black*),

CSF flux (↓ - efflux from the acquisition volume, ↑ - influx into the acquisition volume), fMRI-based CSF signal in slice 1 (*orange*) and slice 2 (*pink*). The pie charts symbolize the saturation state of CSF, being either fully saturated (*white*) and or unsaturated (*black*), the rectangles indicate the signal intensity in the respective slice, which result from mixing of RF-saturated and fresh CSF.